

This is a repository copy of *In-plane/out-of-plane disorder influence on the magnetic anisotropy of Fe<sub>1-y</sub>MnyPt-L10 bulk alloy*.

White Rose Research Online URL for this paper:

<https://eprints.whiterose.ac.uk/101524/>

Version: Accepted Version

---

**Article:**

Cuadrado, R., Liu, Kai, Klemmer, Timothy J. et al. (1 more author) (2016) In-plane/out-of-plane disorder influence on the magnetic anisotropy of Fe<sub>1-y</sub>MnyPt-L10 bulk alloy. Applied Physics Letters. 123102. ISSN 0003-6951

<https://doi.org/10.1063/1.4944534>

---

**Reuse**

Items deposited in White Rose Research Online are protected by copyright, with all rights reserved unless indicated otherwise. They may be downloaded and/or printed for private study, or other acts as permitted by national copyright laws. The publisher or other rights holders may allow further reproduction and re-use of the full text version. This is indicated by the licence information on the White Rose Research Online record for the item.

**Takedown**

If you consider content in White Rose Research Online to be in breach of UK law, please notify us by emailing [eprints@whiterose.ac.uk](mailto:eprints@whiterose.ac.uk) including the URL of the record and the reason for the withdrawal request.

# In-plane/out-of-plane disorder influence on the magnetic anisotropy of $\text{Fe}_{1-y}\text{Mn}_y\text{Pt-L1}_0$ bulk alloy

R. Cuadrado,<sup>1,2</sup> Kai Liu,<sup>3</sup> Timothy J. Klemmer,<sup>4</sup> and R. W. Chantrell<sup>1</sup>

<sup>1</sup>*Department of Physics, University of York, York YO10 5DD, United Kingdom*

<sup>2</sup>*Catalan Institute of Nanoscience and Nanotechnology (ICN2), CSIC and The Barcelona Institute of Science and Technology, Campus UAB, Bellaterra, 08193 Barcelona, Spain*

<sup>3</sup>*Physics Department, University of California, Davis, California 95616, USA*

<sup>4</sup>*Seagate Technology, Fremont, California, 94538, USA*

(Dated: March 7, 2016)

The random substitution of a non-magnetic species instead of Fe atoms in  $\text{FePt-L1}_0$  bulk alloy will permit to tune the magnetic anisotropy energy of this material. We have performed by means of first principles calculations a study of  $\text{Fe}_{1-y}\text{Mn}_y\text{Pt-L1}_0$  ( $y=0.0, 0.08, 0.12, 0.17, 0.22$  and  $0.25$ ) bulk alloy for a fixed Pt concentration when the Mn species have ferro-/antiferromagnetic (FM,AFM) alignment at the same(different) atomic plane(s). This substitution will promote several in-plane lattice values for a fixed amount of Mn. Charge hybridization will change compared to the  $\text{FePt-L1}_0$  bulk due to this lattice variation leading to a site resolved magnetic moment modification. We demonstrate that this translates into a total magnetic anisotropy reduction for the AFM phase and an enhancement for the FM alignment. Several geometric configurations were taken into account for a fixed Mn concentration because of different possible Mn positions in the simulation cell.

The  $\text{FePt-L1}_0$  bulk alloy possesses a high value of magnetocrystalline anisotropy energy (MAE) [1–3] and hence is a promising candidate for next generation ultrahigh density magnetic recording media. The large MAE allows to overcome the superparamagnetic limit [4–6]. Given that high anisotropy media are likely to require Heat Assisted Magnetic Recording to overcome the write field requirement, the low Curie temperature of  $\text{FePt}$  is a further advantage. However, in the manufacturing process, the media must be annealed to transform a face-centered cubic (*fcc*) A1 initial phase into an  $\text{L1}_0$  highly chemically ordered alloy. As was pointed out in some recent experimental and theoretical works, [7–12], introducing into the  $\text{FePt-L1}_0$  alloy magnetic or non-magnetic species such as Ni, Mn or Cu, respectively, permits the reduction of  $T_C$  and control of the MAE values as the Fe concentration decreases.

Initial motivation for the experimental studies was provided by model calculations of Sakuma [13] who investigated the magnetic properties of  $\text{FePt}$  with different levels of band filling  $n_{eff}$  using a fixed band structure model. However, experimental studies [8, 9, 11, 12, 14] achieve variations in  $n_{eff}$  using substitution of Fe sites with impurity atoms such as Ni, Mn, Co, Cr or Cu. Recently [7] we showed that the alloying process itself produces variations in atomic structure and consequent changes in band structure which strongly affect the MAE and saturation magnetization leading to important differences with the fixed band structure approach.

Previously we studied the substitution of the Fe species by Cr, Mn, Co, Ni, or Cu in  $\text{FePt-L1}_0$  bulk alloys keeping the Pt concentration fixed [7]. Here we pursue the effects of the magnetic ordering and also study the variation of the anisotropy of bulk  $\text{FePt-L1}_0$  via the substitution of Fe atoms by diluted Mn, with concentrations much lower than in [7], while keeping Pt fixed. We corre-

late the doping and MAE with the loss of the individual in-plane/out-of-plane value compared to the  $\text{L1}_0$  structure. Cheng-Jun Sun *et al.*, [15] through their proposed model based on directional short range order (DSRO) predicted the decrease of the ordering parameter with increasing Mn doping and hence the structural evolution as a function of  $y$  concentration. To deal with this complex system the ferromagnetic (FM) and antiferromagnetic (AFM) phases of  $\text{FeMnPt-L1}_0$  between different Mn planes have to be studied. We will present a comprehensive analysis of the local range order (LRO) of  $\text{Fe}_{1-y}\text{Mn}_y\text{Pt-L1}_0$  ( $y=0.0, 0.08, 0.12, 0.17, 0.22$  and  $0.25$ ) bulk alloy having several different geometric configurations per fixed Mn:Fe ratio. In the present work, the self-consistent ionic relaxation would not lead in an usual chemical disorder structure since the final geometries maintain the same atomic arrangement in space. We note that in this case, the calculation of the chemical order parameter was not useful because of the bond distances –key values that characterize S– are only slightly different compared to the real disordered material, leading to a S value of 1 for all the studied configurations. We make a direct comparison with theoretical [7, 13] and experimental [8, 9, 15, 16] works on Mn doping, obtaining good qualitative agreement after factoring in the temperature variation.

We have performed density functional theory (DFT) calculations of  $\text{Fe}_{1-y}\text{Mn}_y\text{Pt-L1}_0$  alloys with the SIESTA package [17] using norm-conserving pseudopotentials for the core electrons and the generalized gradient approximation (GGA) for the exchange–correlation energy. MAE is defined as the difference in the total energy between hard and easy magnetization directions and it has been obtained using a fully relativistic (FR) implementation [20] in the GREEN [21] code employing the SIESTA framework.

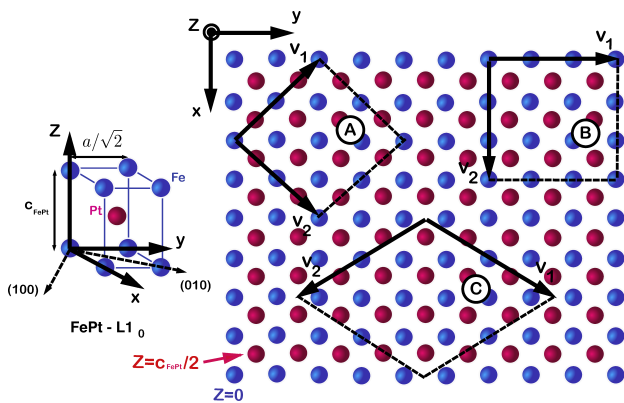


FIG. 1. (Left) Schematic picture of the FePt-L1<sub>0</sub> unit cell and its characteristic lattice values:  $a$  and  $c/a$ . Notice that the in-plane diagonal of the unit cell corresponds to the lattice constant whilst the edge is  $a/\sqrt{2}$ ; (Right) Top view of FePt-L1<sub>0</sub> structure. A, B and C depict three different in-plane lattices with 8, 9 and 12 Fe atoms ( $z=0$ ) and the same number of Pt atoms at  $z=c_{FePt}/2$ . The in-plane lattice vectors employed for each A, B and C supercell sizes are depicted by  $\mathbf{v}_i$ .

On the right side of the figure 1 is shown the schematic in-plane view of three different supercell sizes with 8, 9 and 12 total number of Fe atoms, marked by A, B and C, respectively. We replaced two or four Fe atoms on these different supercells, depending on the desired level of doping, by two or four Mn. Mn was randomly positioned locally within each of the Fe planes and we only applied the constraint that half of the Mn atoms were on each Fe plane. The number of possible different geometric configurations for such systems is quite extensive. However, due to the high symmetry of the simulation supercell we took into account all the necessary geometric configurations for each  $y$  in order to cover, locally, an accurate prediction of their magnetic properties.

We present a detailed study of the structural relaxation and magnetic properties of Mn-doped FePt. As demonstrated previously, the lowest energy configuration for Fe<sub>1-y</sub>Mn<sub>y</sub>Pt-L1<sub>0</sub> alloys corresponds to an antiferromagnetic (AFM) alignment of the Mn atoms between different atomic planes [7, 22]. Consequently we carried out a survey of both FM and AFM phases, imposing the magnetic constraint on the Mn species. However in the present work and since the simulation supercell is bigger, there is a possibility to have another AF alignment of the Mn atoms at the same plane. From now on we will designate the antiparallel alignment with Mn out-of-plane as AFM-1 and that within the same plane AFM-2.

Figure 2 (middle) shows the average total energy values for a fixed Mn concentration ( $y$ ) when its spins are FM, AFM-1 or AFM-2 coupled. It is clear that the AFM phases have lower energy values than FM ones. This result agrees with previous theoretical works [22]. Physically, we can argue that the energy differences between FM, AFM-1 and AFM-2 configurations is mainly due to

two mechanisms: the atomic rearrangement of the species after the ionic relaxation and the subsequent self-consistent electronic configuration. The charge transferred between different species will tend to fill the  $d$  states, making the structures more energetically stable. In our case, as the Mn concentration changes, the  $E_{FM}-E_{AFM}$  values are not constant, having two different ranges:  $\sim 0.22$  eV for  $y \leq 0.12\%$  and  $\sim 0.5$  eV when  $y \geq 0.17\%$ .

The evolution of the lattice parameters  $a$  and  $c/a$  as a function of the Mn concentration is shown in Fig. 2 (right). Due to the Mn substitution, after relaxation, the FePt-L1<sub>0</sub> stacking exhibited in-plane and out-of-plane distortions promoting a set of different in-plane lattice parameters for each geometric configuration and one  $c/a$  value for each. In general, both FM and AFM-1 phases follow the same trend as found in previous studies [7, 16]: as the Mn concentration in FePt-L1<sub>0</sub> bulk increases,  $a$  tends to increase and conversely the out-of-plane  $c/a$  decreases. There is however small discrepancies in  $a$  and  $c/a$  trends for larger concentrations between FM and AFM-1 phases, mainly due to the rearrangement of the valence charge during the ionic optimizations process, leading to more energetically stable structures as well as different bonding distances.

Site resolved magnetic moment (MM) values for FM and AFM-1/-2 phase configurations exhibit different trends as the Mn  $y$  concentration changes in Fe<sub>1-y</sub>Mn<sub>y</sub>Pt-L1<sub>0</sub> alloy, left and right columns in figure 3, respectively. Pt MMs change significantly for the AFM phases, having constant values for FM coupling. This is consistent with the origin of the Pt moment resulting from the Weiss field from the magnetic sublattice [23], which is clearly reduced by the AFM coupling of the Mn atoms. With increasing Mn concentration both types of assumed magnetic order (FM and AFM) present different trends: when Mn atoms are FM aligned the  $MM_{Mn}$  increases, whereas if the Mn spins are AFM aligned the  $MM_{Mn}$  reduce their net values. Consistent with the role of the Fe being to polarize the non-magnetic spins, it is clear for the FM case that, Fe atoms polarize the non-magnetic atoms whilst they do not do so for the AFM case, as in bulk FePt-L1<sub>0</sub> alloy the Fe species do for Pt atoms (at zero Mn concentration).

Thus the proposal of Mryasov et. al. [23] that the non-magnetic atoms are directly polarized by the Weiss field from the Fe seems appropriate on introduction of the Mn impurity atoms. This also allows conjectures relating to the effects of the Mn doping on the MAE. Following Mryasov's theory and the theoretical predictions of Sawatzky *et al* [24], we are able to propose two mechanisms related to the polarization of the non-magnetic species in the MAE values, which will both affect the MAE. On the one hand, the  $MM_{Pt}$  reduction will promote lower Fe-Pt-Fe indirect exchange between the out-of-plane Fe species, and on the other the Mn concentration will induce similar behavior for the direct Fe-Fe exchange interaction, leading to a reduction of the total magnetic anisotropy of the alloy as we will see in figure 4.

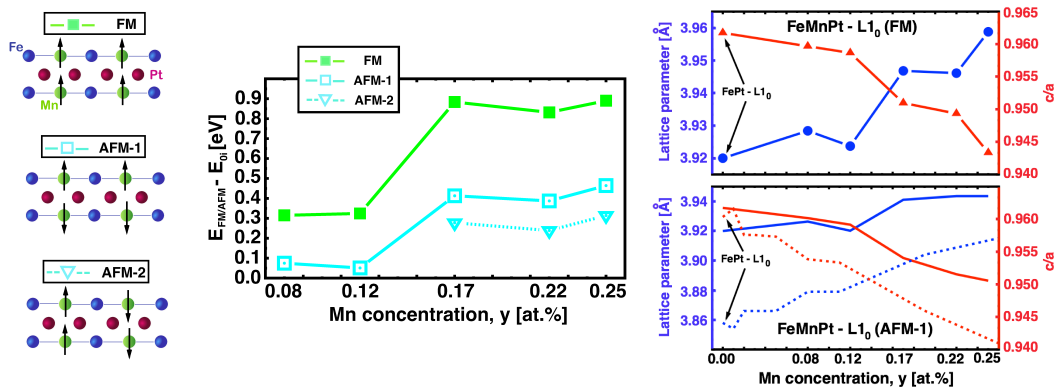


FIG. 2. (Left) Side view of the magnetic alignment between atoms. (Middle) Total energy comparison between ferromagnetic (filled green squares) and antiferromagnetic (empty turquoise squares and invested triangles) phases as the Mn concentration changes from 0.00% up to 0.25%. Each value has been calculated as an average value of several configurations for a fixed Mn concentration as it is shown in the text. The zero energy,  $E_{0i}$ , has set to the minimum value of the energy between all the configurations. The straight lines are guide to the eye. (Right) In-plane lattice constant  $a$  (blue dots) and out-of-plane parameter  $c/a$  (red triangles) as a function of the  $y$  concentration in  $\text{Fe}_{1-y}\text{Mn}_y\text{Pt}$  bulk phases. Blue and red dashed lines depict the experimental dependence of  $a$  and  $c/a$  as shown in the work of Meyer *et al.* [16].

The influence of the Fe substitution with non-magnetic impurities in the FePt-L1<sub>0</sub> bulk alloy promotes changes in its magnetization  $M$  and in the total magnetic anisotropy, increasing for the FM alignment and conversely decreasing for the AFM phases, as shown in the first and second rows in Figure 4 (left/central), respec-

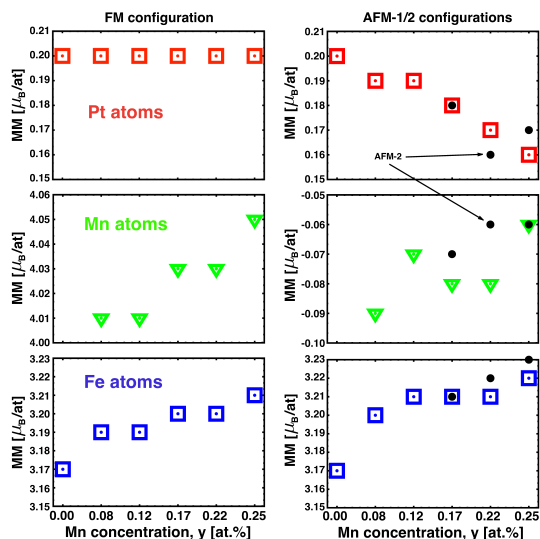


FIG. 3. Magnetic moment values per atom as a function of the Mn concentration  $y$ . On the left column is depicted the FM configurations and on the right those AFM-1/-2. As explained along the text, the MM has been calculated as an average of all the configurations for each concentration. From top to bottom is shown the non-magnetic species, Pt and Mn, red empty squares and green empty triangles, respectively. The site resolved Fe MM values are presented in the last row by empty blue squares. Black dots present the Pt, Mn and Fe MM values for AFM-2 configuration.

tively. As pointed out in [7], each configuration produces a unique band structure, leading to variations in the MAE as represented by the dispersion of the data shown in Figure 4. It can be seen that there is a linear increase (decrease) with the Mn concentration for the FM(AFM) configurations. However the decrease is more marked for the AFM configurations, for which there is also a rapid decrease of the magnetization values with  $y$ . The increase(decrease) of the MAE with the Mn concentration in FM(AFM) structures is a consequence of the change in the electronic structure and hence in the magnetic interactions between different magnetic/non-magnetic atoms. As was pointed out earlier, the physical mechanism to explain the behavior of the MAE in L1<sub>0</sub> alloys is through direct and indirect exchange interactions between in-plane (Fe-Fe) and out-of-plane (Fe-Pt-Fe) neighbors, respectively. So in the AFM cases, there are two complementary ways to explain the reduction in MAE: 1) the reduction in the  $\text{MM}_{\text{Pt}}$  minimizing the out-of-plane indirect exchange interaction and 2) the reduction of the in-plane magnetic interactions due to the fact that the Mn concentration acting as a “magnetic barrier” between Fe species. Specifically for a fixed amount of  $\text{Mn}_y$  in FePt, the dispersion in the MAE changes. Physically, the Mn atoms are located at different Fe sites for each geometric configuration, this will imply the possibility to have not only one in-plane lattice parameter as in FePt-L1<sub>0</sub> but several  $a_i$  depending on whether we have one or more Mn atoms at the same plane. In figure 4 (right) is shown the in-plane lattice distribution function (LDF) that presents the localization of  $a_i$  values around the FePt bulk. For example, in FM/AFM-Fe<sub>0.78</sub>Mn<sub>0.22</sub>Pt (blue dots) the dispersion in the values is 30 meV and inspecting the solid blue line on the right the  $a_i$  values are between 3.8Å and 4.1Å, conversely, for  $y=0.12\%$  (green triangles) the dispersion is smaller and

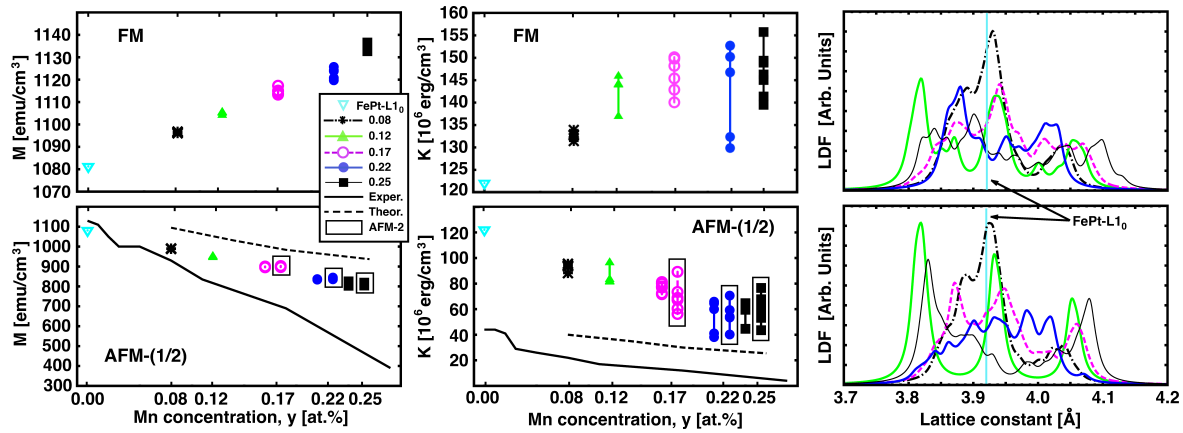


FIG. 4. (Left) Magnetization as a function of the Mn impurities concentration for the FM and AFM-1/-2 alignments. (Middle) Magnetic anisotropy energy (MAE) values as a function of the Mn concentration  $y$  for FM and AFM-1/-2 phases, top and bottom rows, respectively. Each set of the same symbols show different MAE values for a fixed amount of Mn. The additional AFM-2 points are depicted inside black boxes besides their AFM-1 counterparts (Right) In-plane lattice distribution function (LDF) for FM and AFM-1 configurations. Same colors are used for each concentration-LDF. Vertical turquoise line depicts the FePt-L<sub>10</sub> bulk lattice constant. The solid and dashed lines in the Magnetization and MAE graphs depict the experimental results obtained by Meyer *et al.* [16] and those from theory by Suzuki *et al.* [14], respectively.

only three main  $a_i$  peaks localized at 3.82Å, 3.94Å and 4.05Å are depicted.

Finally in Fig. 4, we make a direct comparison with the experimental data of Mn-doped FePt of Meyer *et al.* [16]. At the outset we note that the *ab initio* calculations are zero K values, whereas the experimental values are 300K measurements. This of course leads to a saturation in the magnetization  $M$  and the MAE. In the latter case we note that the MAE as measured is a free energy difference, the reduction with temperature arises from spin fluctuations rather than a change in the MAE at the atomic level. Consider first the saturation magnetization. At low concentration the agreement is good, with the *ab initio* calculations increasingly under-estimating  $M$  under increasing Mn concentration. Here we propose an explanation of this based on the temperature variation of  $M$ . The pure FePt-L<sub>10</sub> phase has a sufficiently high Curie temperature that the reduction in  $M$  from the zero K prediction is rather small, consistent with the results shown in Fig.4. It is likely that the discrepancy between the predicted and experimental  $M$  values arises because of a reduction of  $T_c$  with Mn doping. Although the calculation of the temperature variation of  $M$ , requiring values of the exchange constant  $J$ , is beyond the scope of the current work, Gilbert *et al.* [9] demonstrate experimentally a rapid reduction of  $T_c$  with Cu doping, similarly to the present work. Given that the measurements were made at a constant temperature of 300K, the reduction of  $T_c$  would result in a decrease of the measured  $M$ , consistent with the increasing divergence, with increasing Mn doping, of the calculated and measured  $M$  values in Fig. 4.

Regarding the MAE, the calculated values for the AF ordered phase correctly exhibit the experimental reduc-

tion with increasing Mn doping, albeit with an over-estimated value. Again, this is most likely related to the effects of temperature, coupled with the reduction of  $T_c$ . Mryasov *et al.* [23], using an atomistic model, show that thermal effects lower the MAE by approximately a factor of 2, which would bring the theoretical predictions reasonably close to the experimental values at low Mn doping. However, the thermal reduction in the MAE value would be strongly exacerbated by the reduction in  $T_c$  with increasing Mn doping, consistent with the results shown in Fig. 4.

We have carried out a DFT based study of Fe<sub>1-y</sub>Mn<sub>y</sub>Pt-L<sub>10</sub> bulk phase for  $y=0.08, 0.12, 0.17, 0.22$  and  $0.25$  in their FM and AFM phases. The calculations were carried out by creating the specific alloy structures rather than relying on a fixed band structure model. Due to the Mn substitution, the FePt-L<sub>10</sub> alloy exhibited a set of different in-plane lattice parameters and one out-of-plane value for each configuration. These geometrical changes promote electronic rearrangement and significantly alter the magnetic behavior. From this point of view, average Fe magnetic moments increase in a similar way for both FM and AFM configurations. However non-magnetic species exhibit different trends with the assumed Mn alignment.

A detailed comparison with the experiments of Meyer *et al.* [16] was also made. In general the calculated values showed qualitative agreement with the trend of the experimental values with increasing Mn concentration. Even though the predictions over-estimated the experimental values, it is clear that the AFM phase exhibits fairly good agreements with experiments, while the FM phase shows the opposite trend. It was argued that this enhancement is a result of the temperature reduction of

the MAE.

The authors are grateful to Prof. Chih-Huang Lai for helpful discussions. Financial support of the EU Seventh Framework Programme under Grant No. 281043,

FEMTOSPIN is gratefully acknowledged. K.L. acknowledges support from the US-NSF (DMR-1543582) and the France–Berkeley Fund.

- 
- [1] D. Weller and A. Moser, *IEEE Trans. Magn.*, **36**, 10 (1999).
- [2] C.J. Aas, P.J. Hasnip, R. Cuadrado, E.M. Plotnikova, L. Szunyogh, L. Udvardi, R.W. Chantrell, *Phys. Rev. B*, **88**, 174409, (2013).
- [3] R. Cuadrado and R.W. Chantrell, *Phys. Rev. B*, **89**, 094407, (2014).
- [4] R. Cuadrado and R. W. Chantrell, *Phys. Rev. B* **86**, 224415 (2012).
- [5] P. Gambardella, S. Rusponi, M. Veronese, S. S. Dhesi, C. Grazioli, A. Dallmeyer, I. Cabria, R. Zeller, P. H. Dedrich, K. Kern, C. Carbone, and H. Brune, *Science* **300**, 1130 (2003).
- [6] D. Weller, O. Mosendz, G. Parker, S. Pisana, and T. S. Santos, *Phys. Status Solidi A* **210**, 1245 (2013).
- [7] R. Cuadrado, Timothy J. Klemmer, and R. W. Chantrell, *Appl. Phys. Lett.*, **105**, 152406, (2014).
- [8] D. B. Xu, J. S. Chen, T. J. Zhou, and G. M. Chow, *Appl. Phys. Lett.* **109**, 07B747 (2011).
- [9] Dustin A. Gilbert, Liang-Wei Wang, Timothy J. Klemmer, Jan-Ulrich Thiele, Chih-Huang Lai, and Kai Liu, *Appl. Phys. Lett.* **102**, 132406 (2013)
- [10] D. A. Gilbert, J. W. Liao, L. W. Wang, J. W. Lau, T. J. Klemmer, J. U. Thiele, C. H. Lai, and K. Liu, *APL Mater.* **2**, 086106 (2014).
- [11] B. Wang, K. Barmak, and T. J. Klemmer, *IEEE Trans. Magn.* **46**, 1773 (2010).
- [12] B.Wang, K. Barmak, and T. J. Klemmer, *J. Appl. Phys.* **109**, 07B739 (2011).
- [13] Akimasa Sakuma, *J. Phys. Jap.* **63**, 3053 (1994)
- [14] Takao Suzuki, Hiroshi Kanazawa, and Akimasa Sakuma, *IEEE Trans. Mag.* **38**, 0018 (2002)
- [15] Cheng-Jun Sun, Dongbin Xu, Steve M. Heald, Jingsheng Chen, and Gan-Moog Chow, *Phys. Rev. B* **84**, 140408(R) (2011)
- [16] Gereon Meyer, and Jan-Ulrich Thiele, *Phys. Rev. B* **73**, 214438 (2006).
- [17] J.M. Soler, E. Artacho, J.D. Gale, A. García, J. Junquera, P. Ordejón and D. Sánchez-Portal, *J. Phys.: Condens. Matter*, **14**, 2745, (2002).
- [18] J. P. Perdew, K. Burke and M. Ernzerhof, *Phys. Rev. Lett.*, **77**, 3865, (1996).
- [19] E. Artacho, D. Sánchez-Portal, P. Ordejón, A. García, and J. M. Soler, *Phys. Status Solidi B* **215**, 809 (1999).
- [20] R. Cuadrado and J. I. Cerdá, *J. Phys.: Condens. Matter* **24**, 086005 (2012).
- [21] J.I. Cerdá, M.A. Van Hove, P. Sautet, M. Salmerón, *Phys. Rev. B*, **56**, 15885, (1997).
- [22] Zhihong Lu, Roman V. Chepulskii, and W. H. Butler, *Phys. Rev. B* **81**, 094437 (2010)
- [23] O.N Mryasov, U. Nowak, K.Y. Guslienko and R.W. Chantrell, *Europhysics Letters* **69**, 805 (2005).
- [24] G.A., Sawatzky, W. Geertsma and C. Haas, *J. Mag. Mag. Mat.* **3**, 37 (1976).